ELSEVIER

J. Non-Newtonian Fluid Mech., 68 (1997) 85–100

Journal of Non-Newtonian Fluid Mechanics

On the Peterlin approximation for finitely extensible dumbbells

R. Keunings

Division of Applied Mechanics, Université catholique de Louvain, Bâtiment Euler, B-1348 Louvain-la-Neuve, Belgium

Received 23 May 1996

Abstract

For the simplest non-linear kinetic theory of dilute polymeric solutions (FENE dumbbells), the pre-averaging Peterlin approximation used to derive a macroscopic constitutive equation (FENE-P) is shown to have a significant impact on the statistical and rheological properties of the model. This is illustrated in simulations of transient elongational flows by means of standard and stochastic numerical techniques. © 1997 Elsevier Science B.V. All rights reserved.

Keywords: Constitutive equation; FENE dumbbells; Kinetic theory; Stochastic simulation

1. Introduction

Kinetic theory provides a rational framework for modelling the flow of polymeric liquids [1,2]. It is particularly useful when it yields a constitutive equation for the polymer contribution to the stress tensor that can be used in analytical or computational flow analyses [3]. Unfortunately, it is often necessary to invoke closure approximations in order to derive a constitutive equation from a kinetic model. The impact of these approximations on the rheological response can be significant, both qualitatively and quantitatively [2]. The closure problem also arises in micromechanical theories for suspensions [4].

In the present paper, we address the closure problem for the most elementary non-linear kinetic model of a dilute polymer solution, known as the Warner Finitely Extensible Non-linear Elastic (FENE) dumbbell model [1]. The polymer solution is described as a suspension of non-interacting dumbbells in a Newtonian solvent. Each dumbbell consists of two beads connected by a spring which models intramolecular interactions. As they move through the solvent, the beads experience Brownian motion, Stokes drag and the spring force. For FENE dumbbells, the spring force reads

$$\boldsymbol{F}^{c} = \frac{H}{1 - \boldsymbol{Q}^2/Q_0^2}\,\boldsymbol{Q}, \tag{1}$$

0377-0257/97/$17.00 Copyright © 1997 Elsevier Science B.V. All rights reserved.
PII S0377-0257(96)01497-8

where H is a spring constant, $\boldsymbol{Q}$ is the vector connecting the two beads and Q_0 is the maximum spring length. In the limit of a linear Hookean spring ($Q_0 \to \infty$), it is possible to derive without any closure approximation a constitutive equation for the polymer stress. Together with the Newtonian contribution of the solvent, this yields the classical Oldroyd B model [1]. For finite values of Q_0, however, it is impossible to obtain a constitutive equation that is mathematically equivalent to the FENE theory. The self-consistent pre-averaging approximation due to Peterlin,

$$\boldsymbol{F}^c = \frac{H}{1 - \langle \boldsymbol{Q}^2 \rangle / Q_0^2} \boldsymbol{Q}, \tag{2}$$

yields the FENE-P constitutive equation [5]. In Eq. (2), the angular brackets denote the configuration space average $\langle \cdot \rangle = \int \cdot \psi(\boldsymbol{Q}, t)\, d\boldsymbol{Q}$, where ψ is the distribution function.

It is usually believed that the FENE-P constitutive equation derived from (2) is a good approximation of the FENE kinetic theory, particularly in elongational flows where the distribution of dumbbell configuration can be assumed to be highly localized [6]. The Perterlin approximation is indeed accurate in steady state extension [7,8]. In the present paper, however, we show that such is not the case in time-dependent elongational flows.

Using standard and stochastic numerical techniques, we compare the behaviour of FENE and FENE-P dumbbells in various time dependent extensional flows, i.e. (i) one-dimensional start-up problem, (ii) one-dimensional problem with a time-dependent elongation rate and (iii) inception of uniaxial elongation. We also discuss results for the FENE-CR constitutive equation proposed by Chilcott and Rallison [9]. The latter is a close parent of the FENE-P equation, and it has been used in a number of recent numerical simulations of dilute solutions in complex flows (e.g. [9–12]). The FENE-CR equation is a modified FENE-P model designed to have a constant shear viscosity; it is expected to behave like the FENE-P model in elongation.

The main points made in this paper are as follows.

(i) The Peterlin approximation leading to the FENE-P constitutive equation radically changes the statistical properties of the underlying kinetic theory. The configuration distribution function for FENE-P dumbbells is indeed always Gaussian, and thus never localized, whatever the flow kinematics.

(ii) A direct result of (i) is that nothing prevents individual FENE-P dumbbells from deforming beyond the maximum allowed length Q_0 of the FENE theory. It is only the average $\langle \boldsymbol{Q}^2 \rangle$ that is bounded for FENE-P dumbbells.

(iii) In transient elongational flows, FENE and FENE-P dumbbells exhibit significantly different dynamics of molecular extension and stress. Furthermore, the levels of stress achieved in these time-dependent flows can differ markedly as well.

(iv) As expected, the FENE-P and FENE-CR constitutive equations yield almost identical results in time-dependent elongation.

(v) The stochastic simulation approach is a mathematically sound and accurate alternative to classical numerical techniques for computing viscoelastic stresses. It allows the direct use of kinetic theory models in flow simulations, thereby avoiding the need for mathematical closure approximations whose impact on rheological behaviour can be significant.

Although points (i) and (ii) have already been made in the literature of kinetic theory, notably by Öttinger [13], Wiest et al. [14], Wedgewood and Bird [15] and Wiest and Tanner [16], they appear to have remained unnoticed in the field of computational rheology. In our opinion,

points (i) and (ii) are important, as they imply that results obtained with approximate FENE constitutive models should be treated with caution, should one insist on interpreting them in the framework of the underlying kinetic theory. (Clearly, the approximate FENE constitutive equations are perfectly valid phenomenological models in the framework of continuum mechanics. They could in fact be more successful than (or as limited as) the original FENE kinetic theory in describing experimental data for polymer solutions. We do not address this important issue here).

Points (iii) and (iv) have been made as well by Herrchen and Öttinger [7] in a paper submitted to this journal during the course of our work. (The results presented in Section 4.3 confirm and complement those described in Section 5.6 of [7].) Point (iii) is of obvious importance in the quantitative evaluation of the FENE kinetic theory. Note that a similar conclusion has been drawn by van den Brule [17] in his Brownian dynamics simulations of finitely extensible chains.

Finally, point (v) has been beautifully illustrated by Öttinger [18] in his book on stochastic simulations. At this stage in the development of stochastic techniques for polymeric liquids, however, it remains important to show convincing experimental evidence of their feasibility and numerical accuracy. We hope the present work contributes to this.

The paper is organized as follows. In Section 2, we summarize the FENE kinetic theory, as well as the FENE-P and FENE-CR constitutive equations. The stochastic simulation approach is described in Section 3, while the results are presented in Section 4. Their implications for the analysis of complex polymer flows are briefly discussed in the conclusions.

2. Kinetic theory and constitutive equations

The FENE kinetic theory involves a relaxation time $\lambda_H = \zeta/4H$ and a dimensionless finite extensibility parameter $b = HQ_0^2/kT$, where ζ is the friction coefficient, k is Boltzmann's constant and T is the absolute temperature. In the present paper, we specify $b = 50$ for the sake of illustration. This is within the range of values that are consistent with the underlying kinetic framework, as discussed in [1,7].

All subsequent equations are written in dimensionless form. The connector vector $\boldsymbol{Q}$, the time t and the velocity gradient $\boldsymbol{\kappa}$ are made dimensionless with $(kT/H)^{1/2}$, λ_H and λ_H^{-1} respectively. The magnitude of the dimensionless velocity gradient $\boldsymbol{\kappa}$ can thus be viewed as a Weissenberg number. The polymer stress τ_p is made dimensionless with nkT, where n is the dumbbell number density. Finally, it is convenient to define the following notation:

$$h(x) = \frac{1}{1 - x/b}. \tag{3}$$

The diffusion equation that describes the evolution of the configuration distribution function $\psi(\boldsymbol{Q}, t)$ is then

$$\frac{\partial \psi}{\partial t} = -\frac{\partial}{\partial \boldsymbol{Q}} \cdot \{[\boldsymbol{\kappa}(t) \cdot \boldsymbol{Q} - \tfrac{1}{2}\boldsymbol{F}^c(\boldsymbol{Q})]\psi\} + \frac{1}{2}\frac{\partial}{\partial \boldsymbol{Q}} \cdot \frac{\partial}{\partial \boldsymbol{Q}}\psi. \tag{4}$$

For FENE dumbbells, the dimensionless connector force $\boldsymbol{F}^c$ is given by

$$\boldsymbol{F}^{c}(\boldsymbol{Q}) = h(\boldsymbol{Q}^2)\boldsymbol{Q}, \tag{5}$$

while for FENE-P dumbbells

$$\boldsymbol{F}^{c}(\boldsymbol{Q}) = h(\langle \boldsymbol{Q}^2 \rangle)\boldsymbol{Q}. \tag{6}$$

The link between the statistical distribution of dumbbell configurations and the polymer stress τ_p is provided by Kramers' expression

$$\tau_p = \langle \boldsymbol{Q}\boldsymbol{F}^{c} \rangle - \delta, \tag{7}$$

where δ is the unit tensor. Note that $\tau_p = \mathbf{0}$ at equilibrium.

It is possible to derive from (4) an evolution equation for the covariance tensor $\boldsymbol{A} = \langle \boldsymbol{Q}\boldsymbol{Q} \rangle$:

$$\frac{d\boldsymbol{A}}{dt} - \boldsymbol{\kappa}\cdot\boldsymbol{A} - \boldsymbol{A}\cdot\boldsymbol{\kappa}^{\dagger} = \delta - \langle \boldsymbol{Q}\boldsymbol{F}^{c} \rangle. \tag{8}$$

For FENE dumbbells, the last term of (8) induces a closure problem which makes it impossible to derive an equivalent constitutive equation for τ_p. For FENE-P dumbbells, however, use of the Peterlin approximation (6) closes Eq. (8) as follows:

$$\frac{d\boldsymbol{A}}{dt} - \boldsymbol{\kappa}\cdot\boldsymbol{A} - \boldsymbol{A}\cdot\boldsymbol{\kappa}^{\dagger} = \delta - h[\mathrm{tr}(\boldsymbol{A})]\boldsymbol{A}. \tag{9}$$

Then Kramers' expression (7) becomes

$$\tau_p = h[\mathrm{tr}(\boldsymbol{A})]\boldsymbol{A} - \delta. \tag{10}$$

Eqs. (9) and (10) thus yield a macroscopic constitutive equation for the polymer stress of FENE-P dumbbells [5].

The Peterlin approximation has a profound impact on the statistical character of the distribution function. Indeed, for Gaussian initial conditions, the solution of the diffusion Eq. (4) for FENE-P dumbbells remains Gaussian with zero mean [13]. Within a normalization constant, the FENE-P distribution function is thus given by

$$\psi(\boldsymbol{Q}, t) \propto \exp[-\tfrac{1}{2}\boldsymbol{Q}\cdot\boldsymbol{A}^{-1}(t)\cdot\boldsymbol{Q}]. \tag{11}$$

We shall illustrate this important fact in Section 4.3.

In the present paper, we compare FENE and FENE-P polymer stresses obtained for specified homogeneous kinematics $\boldsymbol{\kappa}(t)$. For FENE dumbbells, one can first solve the diffusion equation (4) for ψ, and then use Kramers' expression (7). Alternatively, one can adopt the stochastic simulation approach, as explained in Section 3. For FENE-P dumbbells, the simplest way is to solve the evolution equation (9) for the covariance tensor, and then to use Kramers' expression (10) for the stress. The stochastic approach, however, can be applied as well.

For completeness, we shall also discuss results obtained with the FENE-CR constitutive equation proposed by Chilcott and Rallison [9]. For the FENE-CR model, the evolution equation for the second moment $\boldsymbol{A}$ reads

$$\frac{d\boldsymbol{A}}{dt} - \boldsymbol{\kappa}\cdot\boldsymbol{A} - \boldsymbol{A}\cdot\boldsymbol{\kappa}^{\dagger} = h[\mathrm{tr}(\boldsymbol{A})](\delta - \boldsymbol{A}), \tag{12}$$

while the polymer stress is given by

$$\tau_p = h[\mathrm{tr}(\boldsymbol{A})](\boldsymbol{A} - \boldsymbol{\delta}). \tag{13}$$

The FENE-CR model is intended to behave like the FENE-P fluid in elongational flow [9].

3. Stochastic simulation

Solving the diffusion equation (4) is mathematically equivalent [18] to solving the following. Itô stochastic differential equation:

$$\mathrm{d}\boldsymbol{Q}_t = \{\boldsymbol{\kappa}(t)\cdot\boldsymbol{Q}_t - \tfrac{1}{2}\boldsymbol{F}^c(\boldsymbol{Q}_t)\}\,\mathrm{d}t + \mathrm{d}\boldsymbol{W}_t, \tag{14}$$

where $\boldsymbol{W}_t$ is the three-dimensional Wiener process (i.e. an idealization of Brownian motion). More precisely, Eq. (14) is an evolution equation for the Markov process $\boldsymbol{Q}_t$, whose probability density ψ is solution to the diffusion equation (4).

In the stochastic simulation approach, one solves (14) numerically for a large number N_d of dumbbells, namely for many individual realizations $\boldsymbol{Q}_t^{(i)}$ of the stochastic process ($i = 1, 2, \ldots, N_d$). Macroscopic observables of interest, such as the polymer stress τ_p or the mean square polymer extension $\mathrm{tr}\langle\boldsymbol{QQ}\rangle$, are then approximated by ensemble averages. For example, the instantaneous polymer stress $\tau_p(t)$ is given by

$$\tau_p(t) \approx \frac{1}{N_d}\sum_{i=1}^{N_d} \boldsymbol{Q}_t^{(i)}\boldsymbol{F}^c(\boldsymbol{Q}_t^{(i)}) - \boldsymbol{\delta}, \tag{15}$$

where either the FENE (5) or the FENE-P (6) spring law is used to evaluate $\boldsymbol{F}^c$. Inspection of (6) shows that an additional ensemble average is necessary to compute $\boldsymbol{F}^c$ for FENE-P dumbbells. The statistical error implied in (15) is of order $N_d^{-1/2}$.

Numerical techniques for solving stochastic differential equations are reviewed in [18,19]. The simplest technique is known as the explicit Euler–Maruyama scheme. Assuming a discretization of the time domain $[t_0, t_{max}]$ with a constant time step Δt, successive approximations of the stochastic process $\boldsymbol{Q}_t$ are obtained using the recurrence

$$\boldsymbol{Q}_{t_{j+1}} = \boldsymbol{Q}_{t_j} + \{\boldsymbol{\kappa}(t_j)\cdot\boldsymbol{Q}_{t_j} - \tfrac{1}{2}\boldsymbol{F}^c(\boldsymbol{Q}_{t_j})\}\Delta t + \Delta\boldsymbol{W}_j, \tag{16}$$

where the vector of Wiener increments $\Delta\boldsymbol{W}_j = \boldsymbol{W}_{t_{j+1}} - \boldsymbol{W}_{t_j}$ has independent Gaussian components with zero mean and variance Δt.

The Euler–Maruyama scheme is of weak order 1. We use it for both FENE and FENE-P dumbbells. Although very simple to implement, it can lead to difficulties with FENE dumbbells. Indeed, if the time step is too large, an individual dumbbell can see its length become larger than the upper bound $b^{1/2}$, at which point the evaluation of the connector force $\boldsymbol{F}^c$ for the next time step leads to unphysical results. A remedy is either to reject such bad moves [18], at the price of decreased numerical accuracy, or to prevent them altogether by using sufficiently small time steps.

For FENE-P dumbbells, the equivalent problem of bad moves leading to unphysical connector forces would be that the ensemble average of dumbbell lengths become larger than $b^{1/2}$ at the end of a time step. We have never encountered this problem in our simulations of

FENE-P dumbbells with the Euler–Maruyama scheme. Of course, and we shall come back to this point, individual FENE-P dumbbells are allowed to have their length go beyond $b^{1/2}$. This is an obvious consequence of the Gaussian character of the FENE-P distribution function (11).

A markedly better numerical technique for FENE dumbbells, proposed by Öttinger [18], is the following semi-implicit predictor–corrector scheme. The predictor is in fact the Euler–Maruyama method (16), which yields $\tilde{\boldsymbol{Q}}_{t_{j+1}}$. The corrector reads

$$[1+\tfrac{1}{4}h(\boldsymbol{Q}^2_{t_{j+1}})\,\Delta t]\boldsymbol{Q}_{t_{j+1}} = \boldsymbol{D}(\boldsymbol{Q}_{t_j}, \tilde{\boldsymbol{Q}}_{t_{j+1}}, \Delta \boldsymbol{W}_j), \tag{17}$$

where the vector $\boldsymbol{D}$ is given by

$$\boldsymbol{D} = \boldsymbol{Q}_{t_j} + \tfrac{1}{2}[\boldsymbol{\kappa}(t_{j+1})\cdot\tilde{\boldsymbol{Q}}_{t_{j+1}} + \boldsymbol{\kappa}(t_j)\cdot\boldsymbol{Q}_{t_j} - \tfrac{1}{2}h(\boldsymbol{Q}^2_{t_j})\boldsymbol{Q}_{t_j}]\,\Delta t + \Delta \boldsymbol{W}_j. \tag{18}$$

The correction $\boldsymbol{Q}_{t_{j+1}}$ is directed along the known vector $\boldsymbol{D}$, while its length is determined from a cubic equation derived from (17). This equation can be shown [18] always to yield a unique solution in $[0, b^{1/2}[$. The predictor–corrector scheme thus completely eliminates the numerical issue of bad moves for FENE dumbbells. Furthermore, it is of weak order 2.

Finally, we note that the Gaussian increments $\Delta \boldsymbol{W}_j$ can safely be replaced by other random variables that are faster to generate. In this work, we use uniformly distributed random increments whose moments are such as to keep unchanged the weak order of the numerical schemes [18].

4. Results

4.1. One-dimensional start-up problem

Let us first consider a one-dimensional problem derived from the general theory of Section 2. We retain only the x or xx component of all variables of interest, namely the velocity gradient $\kappa_{xx}(t) = \partial^u/\partial^x$, the connector Q_x and the polymer stress $\tau_{p,xx}$; all other components are assumed to vanish identically. Since the resulting problem is scalar, we shall drop all reference to the coordinate system, e.g. $Q = Q_x$. Thus, the dumbbells are aligned with equal probability in the positive or negative x direction, and the only effect of the flow field is to change their length.

We specify the following start-up kinematics

$$\kappa(t) = \mathrm{We}\, H(t), \tag{19}$$

where We denotes the Weissenberg number, while $H(t)$ is the Heaviside unit step function. It is assumed that the dumbbells are at equilibrium at $t = 0$, or equivalently that $\tau_p(0) = 0$. The present problem is a one-dimensional cartoon of start-up of uniaxial elongation. We shall see that the corresponding stress response is very similar to that of the actual three-dimensional flow (Section 4.3).

Let us focus on FENE dumbbells first. In view of (5), the one-dimensional version of the diffusion Eq. (4) is

$$\frac{\partial \psi}{\partial t} = -\frac{\partial}{\partial Q}\{[\mathrm{We}\, H(t) - \tfrac{1}{2}h(Q^2)]Q\psi\} + \frac{1}{2}\frac{\partial^2 \psi}{\partial Q^2}, \tag{20}$$

with $|Q| < b^{1/2}$ and $\psi(\pm b^{1/2}, t) = 0$. The equilibrium distribution $\psi_{eq}(Q) \propto h(Q^2)^{-b/2}$ is imposed as initial condition [1]. The full equation (20) cannot be solved analytically. At steady state, however, an exact solution can be found [1], i.e.

$$\psi_{st}(Q) \propto h(Q^2)^{-b/2} \exp(\mathrm{We}\, Q^2), \tag{21}$$

which will serve as a check of the numerical results. Finally, we can note that $\psi(-Q, t) = \psi(Q, t)$.

We have solved the transient problem (20) numerically by means of an explicit central finite difference scheme of first-order accuracy in time and second-order accuracy in space [20]. Numerically converged results, obtained with $\Delta t = 10^{-6}$ and $\Delta Q = b^{1/2}/500$, are shown in Fig. 1 for $\mathrm{We} = 10$ and $b = 50$. The initial transient (until $t \approx 0.1$) exhibits a gradual spread of the distribution function. From $t = 0.1$ on, a very sharp peak develops close to the maximum dumbbell length $b^{1/2} \approx 7.1$. The evolution is particularly fast between $t = 0.1$ and 0.2. A steady state is reached at about $t = 1$. Note in Fig. 1(b) the excellent agreement between the steady-state numerical result and the analytical solution (21).

Having computed the distribution function $\psi(Q, t)$, we can evaluate the relevant time-dependent averages, namely the mean square extension $\langle Q^2 \rangle$ and, through (5) and (7), the polymer stress $\tau_p = \langle h(Q^2) Q^2 \rangle - 1$. These configuration space integrals are computed by means of the trapezoidal rule. The results are shown in Fig. 2, as individual circular symbols. As seen in Fig. 2(a), the mean square extension gradually increases from its equilibrium value of 1 to a steady state that is near the $b = 50$ upper limit. The corresponding stress growth is shown in Fig. 2(b).

Let us now solve the same problem for FENE dumbbells, but with the stochastic approach. The stochastic differential equation equivalent to Eq. (20) is

$$\mathrm{d}Q_t = \{[\mathrm{We}\, H(t) - \tfrac{1}{2} h(Q_t^2)] Q_t\}\, \mathrm{d}t + \mathrm{d}W_t. \tag{22}$$

Fig. 2 shows the results obtained with the semi-implicit scheme (17). The time step is $\Delta t = 10^{-3}$ and the number of realizations is $N_d = 10^4$. We note the excellent agreement between the stochastic results and those obtained from the numerical integration of the diffusion equation. The very small oscillations in the stress curve are indicative of stochastic noise, which can be reduced by increasing N_d.

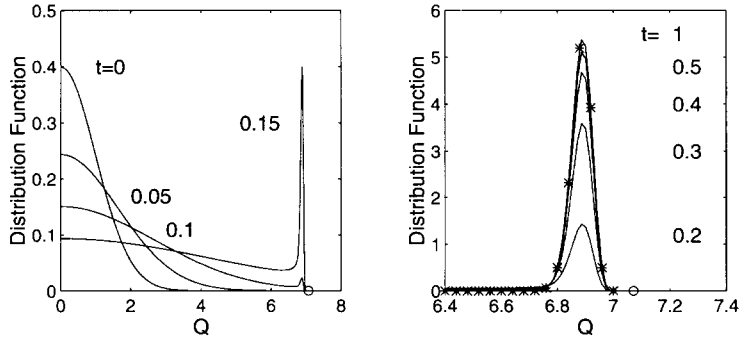

Fig. 1. Distribution function for FENE dumbbells in unidimensional elongation. Finite difference solution of start-up of diffusion equation (20) for $\mathrm{We} = 10$ and $b = 50$. ○ (on the Q axis), upper limit $b^{1/2}$. For $t \geq 0.2$ (right), the distribution function is localized near this limit. *, exact steady-state solution (21).

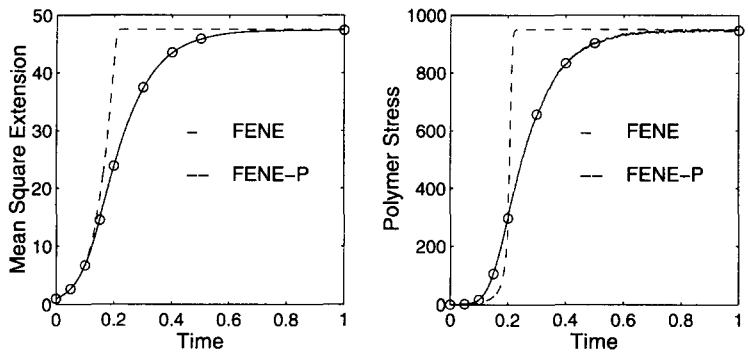

Fig. 2. Temporal growth of mean square extension and polymer stress in start-up of unidimensional elongation (We = 10, $b = 50$): - - -, FENE-P constitutive equation; ——, stochastic results for FENE dumbbells obtained with second-order scheme (17), using $\Delta t = 10^{-3}$ and $N_d = 10^4$; ○, FENE results computed from finite difference solution of diffusion equation (20).

Also shown in Fig. 2 is the behaviour of the FENE-P model under the same flow conditions. In this one-dimensional problem, the evolution equation (9) is scalar and the relevant unknown is $A = \langle Q^2 \rangle$. We solve this equation by means of a fifth-order Runge–Kutta technique with adaptive time stepping. In view of (10), the polymer stress is given by $\tau_p = h(A)A - 1$. Although identical steady states are reached in this problem with the FENE and FENE-P models, the results clearly show that the Peterlin approximation has a significant impact on the transient phase. The mean square extension for the FENE-P model grows faster than for the FENE theory. On the contrary, the FENE-P polymer stress develops more slowly than FENE at earlier times, but then it grows quite sharply to the steady-state plateau.

As an additional check of the numerical accuracy of the stochastic results for FENE dumbbells, we show in Fig. 3 the distribution of dumbbell configurations as a function of time. The normalized histograms are drawn directly from the stochastic simulation, while the continuous curves correspond to the finite difference solution of the diffusion equation (20). The agreement between the two approaches is excellent.

Finally, Fig. 4 illustrates the reduction of statistical errors with an increasing number of realizations. We focus on the solution at $t = 0.15$, and compare again the stochastic and finite difference results. Although the stochastic results with $N_d = 100$ are poor, convergence with increasing N_d is observed. The corresponding averages are compared with their finite difference counterparts in Table 1. We also give estimates [18] of the statistical errors $\epsilon_{stat} = [\mathrm{Var}(X)/N_d]^{1/2}$, where X is either Q^2 or $h(Q^2)Q^2$. Convergence of the stochastic results is consistent with the expected $N_d^{-1/2}$ behaviour.

4.2. One-dimensional complex flow

The above results show that the Peterlin approximation has a dramatic impact on the dynamics of molecular extension and stress. We illustrate this point further for a more complex one-dimensional flow. Instead of the simple start-up kinematics (19), we specify the following time-dependent velocity gradient:

$$\kappa(t) = \begin{cases} 100t(1-t)\exp(-4t) & \text{for } 0 \le t \le 1 \\ 0 & \text{otherwise.} \end{cases} \tag{23}$$

Fig. 5 illustrates the evolution of the velocity gradient $\kappa(t)$, which can be viewed as an instantaneous Weissenberg number. We have $\kappa_{max} \approx 7.2$ at $t \approx 0.2$.

Fig. 6 shows the simulation results for the FENE, FENE-P and FENE-CR models, with $b = 50$. We specify the equilibrium state as initial condition. The FENE results have been computed by means of the semi-implicit stochastic scheme (17), with $\Delta t = 10^{-2}$ and $N_d = 10^4$. Another simulation with $\Delta t = 10^{-3}$ and $N_d = 10^5$ produced identical results at the scale of the drawing. For the FENE-P and FENE-CR models, we have integrated the scalar moment equations derived from (9) and (12) with the kinematics (23), using an adaptive fifth-order Runge–Kutta technique. This yields the second moment A, which is used in the scalar versions of (10) and (13) to compute the polymer stress τ_p. Inspection of Fig. 6 confirms the significant impact of the Peterlin approximation in transient problems. The very sharp growth dynamics of the FENE-P model allow it to reach high levels of mean square extension before the relaxation process takes over. As a result, the FENE-P stress increases quickly, to more than twice the FENE stress at $t \approx 0.4$, before decaying eventually to zero. For the FENE model, the mean square extension grows more slowly, and the large values of the instantaneous Weissenberg number are unable to deform the dumbbells significantly before relaxation sets in. As in the start-up flow of Section 4.1, the FENE stress develops faster than the FENE-P in the beginning of the growth process. Finally, Fig. 6 shows that the FENE-P and FENE-CR models behave identically. This is expected since the present one-dimensional problem is an extensional flow.

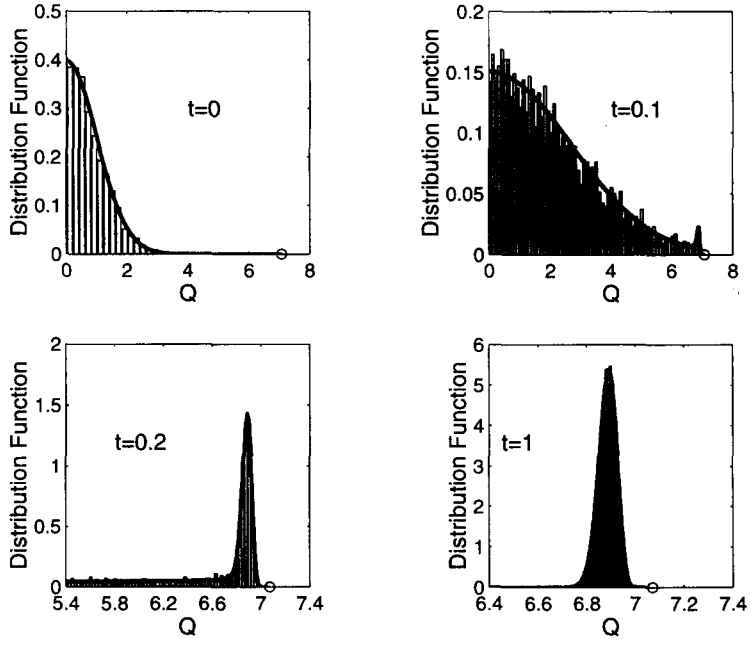

Fig. 3. Distribution function for FENE dumbbells in start-up of unidimensional elongation (We = 10, $b = 50$): ——, finite difference solution of diffusion equation (20); histograms, stochastic simulation with second-order scheme (17) using $\Delta t = 10^{-3}$ and $N_d = 10^4$. ○ (on the Q axis), upper limit $b^{1/2}$; for $t \ge 0.2$, the distribution function is localized near this limit.

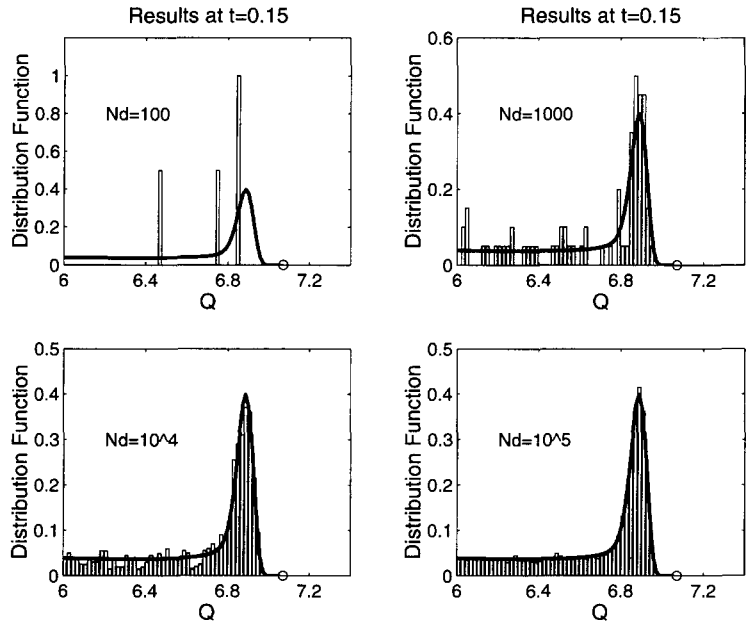

Fig. 4. Distribution function at $t = 0.15$ for FENE dumbbells in start-up of unidimensional elongation (We = 10, $b = 50$): ——, finite difference solution of diffusion equation (20); histograms, stochastic simulation using the second-order scheme (17), with $\Delta t = 10^{-3}$ and N_d ranging between 100 and 10^5. ○ (on the Q axis), upper limit $b^{1/2}$.

Table 2 illustrates the numerical convergence of the first- and second-order stochastic techniques as the time step is decreased. Here, we focus on the mean square extension of FENE dumbbells computed at $t = 0.45$ with $N_d = 10^4$. The superiority of the second-order scheme is evident. From the N_d realizations of Q^2, we find that the statistical error is about 0.17. As observed in Table 2, it is unproductive in this problem to use the second-order scheme with a time step smaller than 10^{-2} (while keeping N_d unchanged), since the temporal discretization errors are then of the same magnitude as the statistical error.

Table 1
Mean square extension and polymer stress at $t = 0.15$ in start-up of unidimensional elongation (We = 10, $b = 50$)

N_d	Extension	ϵ_{stat}	Stress	ϵ_{stat}
10^2	13.4	1.5	79	27
10^3	14.0	0.5	103	8
10^4	14.3	0.2	102.7	3
10^5	14.48	0.05	105.8	0.8
FD	14.47		105.55	

Stochastic results for FENE dumbbells, obtained with second-order scheme (17) using $\Delta t = 10^{-3}$ and increasing values of N_d. The corresponding statistical errors ϵ_{stat} are estimated from the N_d realizations. The last line gives the reference results computed from the finite difference solution of the diffusion equation (20).

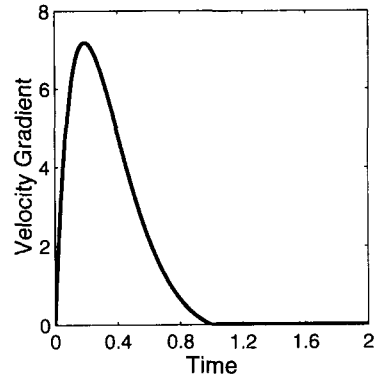

Fig. 5. Velocity gradient (23) specified in unidimensional complex flow.

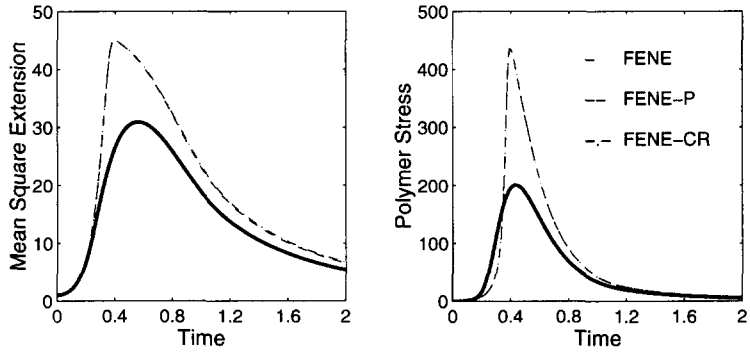

Fig. 6. Temporal evolution of mean square extension and polymer stress in unidimensional complex flow ($b = 50$): - - -, FENE-P constitutive equation; —·—, FENE-CR constitutive equation; —— stochastic results for FENE dumbbells obtained with second-order scheme (17), using $\Delta t = 10^{-2}$ and $N_d = 10^4$. At the scale of this drawing, FENE-P and FENE-CR results are identical.

Finally, we wish to point out that the levels of dumbbell extension and polymer stress reached in this time-dependent problem are smaller than what would be obtained under steady state conditions for the same values of the instantaneous Weissenberg number. Consider for example the FENE-P model, and let us compute what would be the steady state stress τ_p^{st} obtained for

Table 2
Mean square extension of FENE dumbbells in unidimensional complex flow ($b = 50$)

Δt	First order	Second order
10^{-2}	27.0	28.9
10^{-3}	28.6	29.0
10^{-4}	28.9	29.1
10^{-5}	28.9	29.2
10^{-6}	29.1	—

Results at $t = 0.45$, obtained by means of the first- and second-order schemes (16) and (17) respectively ($N_d = 10^4$).

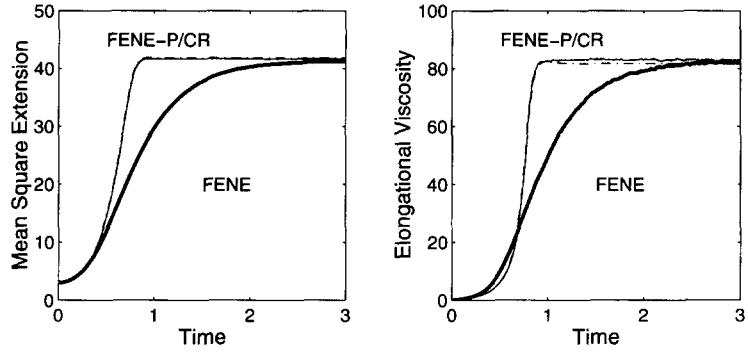

Fig. 7. Temporal evolution of mean square extension and polymer contribution to the elongational viscosity in start-up of uniaxial elongation (We = 3, $b = 50$): ---, FENE-P constitutive equation; – · –, FENE-CR constitutive equation; ——, stochastic results for FENE dumbbells obtained with second-order scheme (17), using $\Delta t = 10^{-2}$ and $N_d = 10^4$; ——, stochastic results for FENE-P dumbbells obtained with first-order scheme (16), using $\Delta t = 10^{-2}$ and $N_d = 10^4$.

$\kappa_{max} = 7.2$. We find $\tau_p^{st} = 670$, which is about 1.5 times larger than the maximum FENE-P stress computed in the transient experiment (Fig. 6).

4.3. Start-up of uniaxial elongation

Lastly, we consider the three-dimensional flow problem of inception of uniaxial elongation. In Cartesian coordinates, the specified kinematics are

$$\boldsymbol{\kappa}(t) = \mathrm{We}\, H(t)\, \mathrm{diag}(-\tfrac{1}{2}, -\tfrac{1}{2}, 1), \tag{24}$$

and the polymer stress has the form $\tau_p = \mathrm{diag}(\tau_{p,xx}, \tau_{p,yy}, \tau_{p,zz})$ with $\tau_{p,xx} = \tau_{p,yy}$. At $t = 0$, we specify the equilibrium state. The observables of interest are the mean square extension, $\mathrm{tr}\langle \boldsymbol{QQ} \rangle$ and the dimensionless polymer contribution to the time-dependent elongational viscosity $\bar{\eta}^+ = (\tau_{p,zz} - \tau_{p,xx})/\mathrm{We}$.

The simulations are for We = 3 and $b = 50$. The FENE results have been computed by means of the semi-implicit stochastic scheme (17), with $\Delta t = 10^{-2}$ and $N_d = 10^4$. Identical results have been obtained with the Euler–Maruyama technique, but at the expense of a smaller time step (i.e. $\Delta t = 10^{-3}$) so as to avoid the issue of bad moves (Section 3).

For the FENE-P and FENE-CR models, we have integrated the moment equations (9) and (12) with the kinematics (24), using an adaptive fifth-order Runge–Kutta technique. This yields the second moment $\boldsymbol{A}$, which is used in (10) and (13) to compute the elongational viscosity. As yet another check of the stochastic approach, we have also solved the stochastic differential equation (14) with the FENE-P spring law (6). This is achieved using the Euler–Maruyama scheme with $\Delta t = 10^{-2}$ and $N_d = 10^4$.

As seen in Fig. 7, the results for the FENE and FENE-P models are qualitatively identical to those obtained in Section 4.1 for the one-dimensional start-up flow (cf. Fig. 2). In particular, the Peterlin approximation greatly alters the dynamics of the mean square extension and of the polymer stress. Fig. 7 also shows that the FENE-P and FENE-CR models behave very similarly,

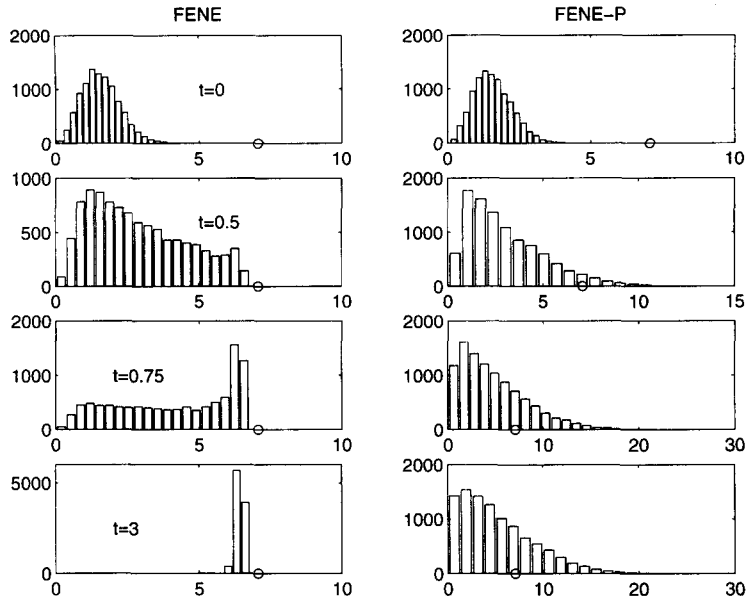

Fig. 8. Distribution of dumbbell length in start-up of uniaxial elongation (We = 3, $b = 50$): FENE dumbbells, stochastic simulation with second-order scheme (17); FENE-P dumbbells, stochastic simulation with first-order scheme (16); both simulations use $\Delta t = 10^{-2}$ and $N_d = 10^4$. Results shown in the form of raw (i.e. unnormalized) histograms of dumbbell length. The vertical axis is the number of events in each bin, while the horizontal axis is the dumbbell length. ○ (on horizontal axis), FENE limit $b^{1/2}$. Note that many individual FENE-P dumbbells have passed this limit. The steady state is essentially achieved at $t = 3$ (see also Figs. 9 and 10).

which is expected in elongational flow. Finally, we note that the above results confirm the recent computations of Herrchen and Öttinger [7], as can be seen by comparing their Fig. 11(b) with 7(b).

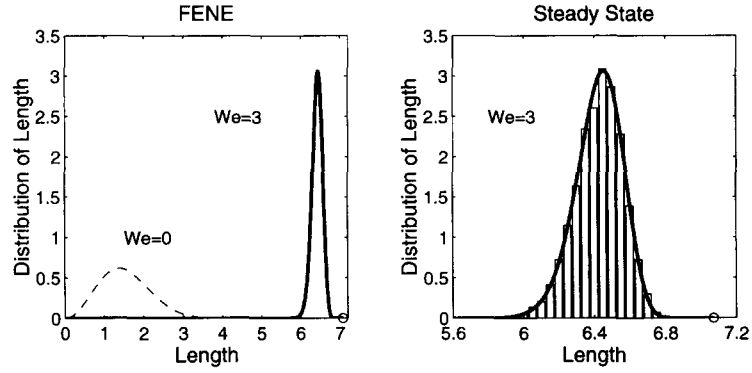

Fig. 9. Steady state distribution of length for FENE dumbbells in uniaxial elongation (We = 3, $b = 50$): ——, computed from exact solution (25); - - -, equilibrium distribution; normalized histograms (right), stochastic simulation with second-order scheme (17) and $N_d = 10^4$; ○ (on horizontal axis), upper limit $b^{1/2}$.

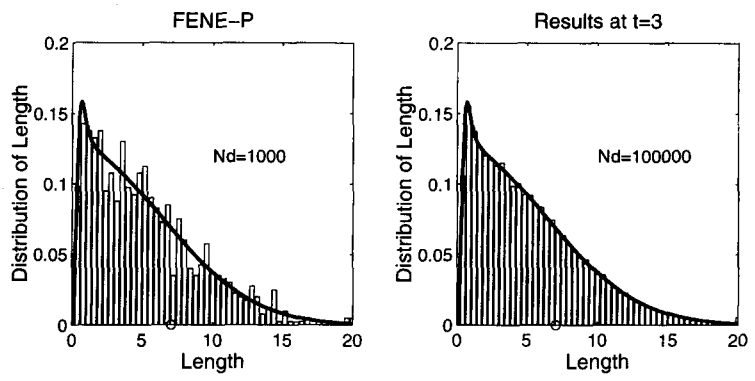

Fig. 10. Distribution of length at $t = 3$ for FENE-P dumbbells in uniaxial elongation (We = 3, $b = 50$): ——, reference solution obtained by solving the moment equation (9); normalized histograms, stochastic simulation with first-order scheme (16), with $N_d = 10^3$ and 10^5. ○ (on horizontal axis), FENE limit $b^{1/2}$. Note that many individual FENE-P dumbbells have passed this limit.

Additional insight into the Peterlin approximation can be gained from Fig. 8, where we compare the evolution of the radial distribution (i.e. the distribution of dumbbell length) for the FENE and FENE-P models. These results are readily obtained from the stochastic simulations, in the form of histograms of the N_d realizations of $(\boldsymbol{Q}_t^2)^{1/2}$. Starting from the equilibrium state, the radial distribution for the FENE dumbbells evolves in time towards a highly extended steady state, localized near the $b^{1/2} \approx 7.1$ upper limit. The FENE-P dumbbells behave in a very different manner. Indeed, many individual dumbbells do cross the $b^{1/2}$ limit as they are deformed by the flow field. Moreover, the steady-state radial distribution is drastically different from that obtained with the FENE dumbbells. These observations are consistent with the Gaussian character (11) of the FENE-P distribution function.

An independent check of the accuracy of the FENE results is provided by the available analytical solution [1] for the steady-state configuration distribution function. In terms of the spherical coordinates (Q, θ, ϕ), we have

$$\psi_{st}(\boldsymbol{Q}) \propto h(Q^2)^{-b/2} \exp[-\tfrac{1}{2}\mathrm{We}\, Q^2(1 - 3\cos^2\theta)]. \tag{25}$$

The exact result for the FENE steady-state radial distribution is then obtained by contracting (25):

$$\psi_{st}^{rad}(Q) \propto Q^2 \int_0^{\pi} \psi_{st} \sin\theta \, d\theta. \tag{26}$$

We compute this integral by the trapezoidal rule. The analytical solution (26) is compared with the stochastic simulation result in Fig. 9. The agreement is excellent.

Finally, the FENE-P stochastic results can also be checked as follows. Since the FENE-P distribution function $\psi(\boldsymbol{Q}, t)$ is Gaussian with zero mean, it can be fully determined through (11) once its second moment $\boldsymbol{A}(t)$ is known. We compute the latter by means of an adaptive fifth-order Runge–Kutta integration of the moment equation (9). We thus obtain the distribution function, which is then contracted as in (26). This yields the transient FENE-P radial

distribution function, which can be compared with the stochastic results. Excellent agreement is found throughout the transient process. For example, we show in Fig. 10 the comparison at $t = 3$ for two stochastic simulations with $N_d = 10^3$ and 10^5; the time step is $\Delta t = 10^{-2}$. The good accord for $N_d = 10^3$ is notable; statistical errors are significantly reduced in the refined simulation with $N_d = 10^5$.

5. Conclusions

Our main conclusions having already been given in the introductory section, we only wish to add that the present results, obtained for specified homogeneous kinematics, are relevant to more complex flow situations. Indeed, in a complex flow field, the polymer molecules experience a time-dependent velocity gradient (at least in the Lagrangian sense) as they are convected along the flow trajectories. We thus expect drastic differences in simulations of complex flows between the FENE kinetic theory and its approximate FENE-P version. This is indeed what is observed in recent simulations of FENE dumbbells in flows between eccentric rotating cylinders [21,22].

As discussed by Öttinger [18], the stochastic simulation approach can be applied to more sophisticated kinetic models of polymer solutions and melts. It is hoped that the direct use of kinetic models in flow simulations, made possible by the stochastic approach, will bring more insight into the rheological behaviour of polymeric liquids.

Acknowledgments

I wish to thank R.B. Bird, P. Halin, M. Laso, H.C. Öttinger, J.D. Schieber and B.H.A.A. van den Brule for their helpful comments. This work has been performed while on sabbatical leave at the University of Cambridge (UK), as visitor at the Department of Applied Mathematics and Theoretical Physics, and as participant in the research programme Dynamics of Complex Fluids of the Isaac Newton Institute for Mathematical Sciences. I wish to thank my hosts E.J. Hinch and J.M. Rallison (DAMTP), and J.R.A. Pearson, K. Walters and T.C.B. McLeish (INIMS), for their kind hospitality and a very stimulating environment.

References

[1] R.B. Bird, C.F. Curtiss, R.C. Armstrong and O. Hassager, Dynamics of Polymeric Liquids, Vol. 2: Kinetic Theory, Wiley, New York, 2nd edn., 1987.
[2] R.B. Bird and H.C. Öttinger, Annu. Rev. Phys. Chem., 43 (1992) 371–406.
[3] R.B. Bird and J.M. Wiest, Annu. Rev. Fluid Mech., 27 (1995) 169–193.
[4] A.J. Szeri and L.G. Leal, J. Fluid Mech., 242 (1992) 549–576.
[5] R.B. Bird, P.J. Dotson and N.L Johnson, J. Non-Newtonian Fluid Mech., 7 (1980) 213–235.
[6] R.I. Tanner, Engineering Rheology, Clarendon, Oxford, 1985.
[7] M. Herrchen and H.C. Öttinger, J. Non-Newtonian Fluid Mech., submitted November 1995.
[8] J.M. Kobe and J.M. Wiest, J. Rheol., 37 (1993) 947–960.
[9] M.D. Chilcott and J.M. Rallison, J. Non-Newtonian Fluid Mech., 29 (1988) 381–432.

[10] P. Singh and L.G. Leal, Theor. Comput. Fluid Dyn., 5 (1993) 107–137.
[11] J.V. Satrape and M.J. Crochet, J. Non-Newtonian Fluid Mech., 55 (1994) 91–111.
[12] O.G. Harlen, J.M. Rallison and P. Szabo, J. Non-Newtonian Fluid Mech., 60 (1995) 81–104.
[13] H.C. Öttinger, J. Non-Newtonian Fluid Mech., 26 (1987) 207–246, Appendix A.
[14] J.M. Wiest, L.E. Wedgewood and R.B. Bird, J. Chem. Phys., 90 (1989) 587–594.
[15] L.E. Wedgewood and R.B. Bird, Ind. Eng. Chem. Res., 27 (1988) 1313–1320.
[16] J.M. Wiest and R.I. Tanner, J. Rheol., 33 (1989) 281–316.
[17] B.H.A.A. van den Brule, J. Non-Newtonian Fluid Mech., 47 (1993) 357–378.
[18] H.C. Öttinger, Stochastic Processes in Polymeric Fluids: Tools and Examples for Developing Simulation Algorithms, Springer, Berlin, 1996.
[19] P.E. Kloeden and E. Platen, Numerical Solution of Stochastic Differential Equations, Springer, Berlin, 1992.
[20] K.W. Morton and D.F. Mayers, Numerical Solution of Partial Differential Equations, Cambridge University Press, Cambridge, 1994.
[21] P. Halin and R. Keunings, Evaluation of the stochastic approach for computing viscoelastic stresses in complex flows, in preparation (1996).
[22] M. Laso, M. Picasso and H.C. Öttinger, Two-dimensional, time-dependent viscoelastic flow calculations using CONNFFESSIT, submitted to AICLEJ. (1996).